Title

Unveiling Highly Sensitive Active Site in Atomically Dispersed Gold Catalysts for Enhanced Ethanol Dehydrogenation

Journal

Angewandte Chemie, 136(35)

ISSN

0044-8249

Authors

Yang, Ji

Zheng, Juan

Dun, Chaochao

et al.

Publication Date

2024-08-26

DOI

10.1002/ange.202408894

Unveiling Highly Sensitive Active Site in Atomically Dispersed Gold Catalysts for Enhanced Ethanol Dehydrogenation

Ji Yang[a,b,c†], Juan Zheng[b†], Chaochao Dun[c†], Lorenz J. Falling[d], Qi Zheng[e], Jeng-Lung Chen[f], Miao Zhang[g], Nicholas R. Jaegers[g], Chithra Asokan[g], Jinghua Guo[d], Miquel Salmeron[e], David Prendergast[c], Jeffrey J. Urban[c*], Gabor A. Somorjai[g*], Yanbing Guo[b*], Ji Su[a*]

[a] Dr. J. Yang, Dr. J. Su
Energy Storage and Distributed Resources Division
Lawrence Berkeley National Laboratory
Berkeley, California 94720, United States
E-mail: jisu@lbl.gov

[b] Dr. J. Yang, Juan Zheng, Prof. Y. Guo
College of Chemistry,
Central China Normal University
Wuhan 430079, People's Republic of China
E-mail: guoyanbing@mail.ccnu.edu.cn

[c] Dr. J. Yang, Dr. C. Dun, Dr. D. Prendergast, Dr. J. J. Urban
The Molecular Foundry
Lawrence Berkeley National Laboratory
Berkeley, California 94720, United States
E-mail: jjurban@lbl.gov

[d] Dr. L. J. Falling, Dr. J. Guo
Advanced Light Source
Lawrence Berkeley National Laboratory
Berkeley, California 94720, United States

[e] Q. Zheng, Prof. M. Salmeron
Materials Science Division
Lawrence Berkeley National Laboratory
Berkeley, California 94720, United States

[f] Dr. J. Chen
National Synchrotron Radiation Research Center, Science-Based Industrial Park
Hsinchu 30076, Taiwan

[g] Dr. M. Zhang, Dr. N. R. Jaegers, Dr. C. Asokan, Prof. G. A. Somorjai
College of Chemistry
University of California-Berkeley
Berkeley, California 94720, United States
E-mail: somorjai@berkeley.edu

†These authors contributed equally to this work.

Supporting information for this article is given via a link at the end of the document.

Abstract: Catalyst design by considering single metal atoms with the surrounding metal and functional species on supports as a sensitive "reaction pool" is a feasible way to find right ethanol-dehydrogenation catalysts. Herein, by inserting single Au atom in four representative metal oxide supports (ZrO_2, CeO_2, TiO_2 and Al_2O_3) as prototypes of catalytic centers, we studied the effects of ensemble pool sites (EPS) composed of Au atom and different surrounding metal atoms and functional species on catalyzing ethanol dehydrogenation. The EPS of Au, Oxygen Vacancy (Vo), and Zr^{3+} or Ce^{3+} favorably formed in Au_1/ZrO_2 or Au_1/CeO_2 facilitates ethanol dehydrogenation to acetaldehyde and ethyl acetate. Au_1/TiO_2 exhibited exclusive formation of acetaldehyde, probably due to confined local space of Au-Ti EPS created by Au atom immobilization preferentially at Vo. While Au_1/Al_2O_3 formed by localizing Au atom on surface hydroxyl group, lacks ensemble pool synergistic site and favors ethanol dehydration to generate diethyl ether. Moreover, the dehydrogenation rate over Au_1/ZrO_2 reaches above 37,964 mol H_2 per mol Au per hour (385 g H_2 g_{Au}^{-1} h^{-1}) at 350 °C, which is 3.32, 2.94 and 15 times higher than those for Au_1/CeO_2, Au_1/TiO_2, and Au_1/Al_2O_3, respectively. The insights from in-situ DRIFTS, APXPS, and DFT calculations allow us to determine that the specific ensemble pool synergy between Au and Vo-Zr^{3+}, changed the rate-determining step and induced kinetically and thermodynamically favorable elementary steps, thus resulting in highly efficient and selective ethanol dehydrogenation. The concept of EPS engineering and synergistic-site preparation methods presented here sheds

new lights for the rational design of ethanol-dehydrogenation catalysts.

Introduction

Hydrogen is a powerful vector of energy and will be vital for a successful energy transition toward carbon neutrality.[1] The development of hydrogen energy technology necessitates cost-effective and energy-efficient H_2 storage and transport methods. Bio-ethanol, produced from bio-mass (such as cassava, cellulose) upgrading, represents an attractive liquid organic hydrogen carriers (LOHC) alternative to store hydrogen in chemical bonds and transport H_2 in liquid molecules due to its renewability, environmental friendliness, and mild operation process of dehydrogenation and hydrogenation cycles.[2,3] A viable bio-ethanol-LOHC system requires a highly efficient and selective catalyst to release impurity-free H_2 from ethanol dehydrogenation.

The last decade has seen the emergence of a new concept in heterogeneous catalysis, based on the synthesis of atomically dispersed catalysts (ADCs), where single metal atoms, usually noble metals, are covalently anchored on an oxide support that immobilizes and prevents them from sintering.[4,5] Reduction of the size of metal nanoparticles down to a single atom achieves the maximum utilization efficiency of expensive metals and uniform distribution of active sites, simultaneously benefiting from gains in activity, stability and selectivity.[6–8] The interactions among single atoms and matrix oxides involve similar phenomena of charge transfer and species spillover on the surrounding support that are the basis of the long-established strong metal-support interaction (SMSI),[5,9] where the active sites are thought to be the interface or perimeter atoms of the nanoparticle in contact with the oxide support.[10] The mono-atomicity of the ADCs provides a bridge between homogeneous metal complexes, single atom, clusters, and nanoparticle catalysts.[11–17] This also offers us the opportunity to develop desirable catalysts to achieve highly efficient and selective ethanol dehydrogenation at reduced cost. Furthermore, the MSI of the ADC becomes incredibly important, not only because the electronic properties and the catalytic performance are largely, or even chiefly, dependent on it,[18] but also the oxygen vacancies, coordinately unsaturated metal ions, or other atoms in the local environment of single metal site can contribute as an active center and create synergies with single metal atom, to further facilitate chemical reactions. Our previous studies demonstrated that the immobilization of single Pt atom onto reducible CeO_2 support generates super-synergy effects between Pt atom and its surroundings, which cooperatively facilitates the adsorption, activation, reaction and desorption of the reactant, intermediates, and products.[19–23] The most recent studies also show that combining a single metal atom with oxygen vacancies and surrounding metal ion on supports can enhance the reaction rate and control the desired product selectivity.[24,25] Therefore, considering the single metal atom and surrounding species as a set of new active sites and further revealing their coordination microenvironment effects becomes a new frontier direction toward the design and manufacture of advanced heterogeneous catalysts [5,9].

The coordination microenvironment of these combined active sites depends on the interaction of single metal atom with the support. Previous studies have demonstrated that single metal atoms could be isolated on oxide solid supports in the form of surface functional groups or electrostatic interactions stabilized single atoms,[26–29] anion defect-anchored single atoms,[30–38] or cation vacancy-embedded single atoms.[39–50] These isolations create various coordination microenvironment of single atoms which mainly depends on the reducibility of solid supports. For example, irreducible oxides such as Al_2O_3 are known to adsorb/support Ag, Rh, and Pt single atoms by terminal surface hydroxyl(-OH)/lattice oxygen (O^{2-}) binding.[26–28] For a reducible support, the single metal atom could be adsorbed on the oxide surface by electrostatic interactions, depending on the synthetic approach used.[4,51] More generally, the single metal atoms are strongly coordinated onto redox support and located at anion defects or cation vacancies through atom migration induced by surface reconstruction. For example, in contrast to CeO_2- [19–23,49,52] or ZrO_2-[41,50] based catalysts where Au sites are usually stabilized by defective O binder, Au atom will occupy the oxygen vacancy and create an Au-Ti complex on TiO_2[30,31,37,52] due to favorable thermodynamics, which has been confirmed both theoretically and experimentally. In addition, the coordination microenvironment effects are also influenced by the arrangement of combined active atoms and the bonding with the intermediate during the reaction. For example, the immobilization of single metal atoms on a reducible support such as CeO_2, will create more oxygen vacancies and undercoordinated Ce^{3+}.[19–23] Previous studies have demonstrated that the surface Ce^{3+} are Lewis acidic sites and the neighboring surface lattice oxygen are Lewis basic sites, and this solid frustrated Lewis pair structure has been demonstrated to promote the adsorption and activation of reactants such as H_2 and CO_2.[53–56] During the reaction, especially a reaction involving H species, H will bond with single metal atom and/or the undercoordinated metal ion on support to generate metal hydrides, which not only enlarge the coordination number of these metals, but also regulate the acid/base properties. For example, the creation of Ce-H species which has been observed through neutron scattering and Raman spectroscopies[57,58], has been demonstrated to improve dehydrogenation/hydrogenation process.[59–62] Therefore, studying the ensemble effect of the combined active sites of ADCs and their catalysis synergy on the chemical reaction is critical for understanding their

structure-function relationships and finding the right ethanol dehydrogenation catalyst.

In this work, we prepared four representative ADCs samples by loading single Au atoms on ZrO_2, CeO_2, TiO_2 and Al_2O_3 supports. The combined active sites of Au atom and its surroundings in these ADCs are referred to Au-ensemble pool sites (EPS). By employing ethanol dehydrogenation as a model reaction, we probed Au-EPS effects of four ADCs on ethanol dehydrogenation. In situ diffuse reflectance infrared transform spectroscopy (DRIFTS), ambient-pressure X-ray photoelectron spectroscopy (APXPS), and density functional theory (DFT) calculations were employed to study the synergistic effect of Au-Vo-Zr^{3+} as highly-sensitive ensemble pool sites on ethanol dehydrogenation over Au_1/ZrO_2.

Results and Discussion

The formation of various Au-ensemble pool sites

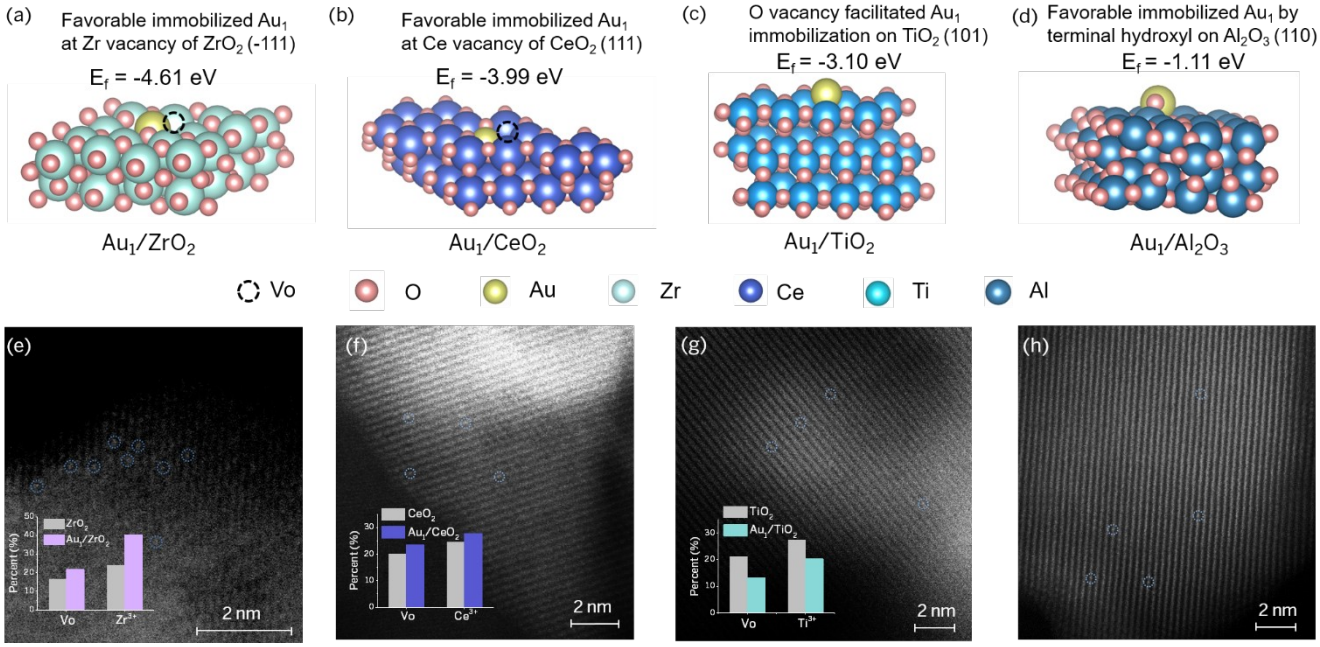

Figure 1. The optimized structure of four ADC prototypes. DFT models of Au atom on various oxide supports: (a) Zr vacancy immobilized Au_1 on ZrO_2 (-111), (b) Ce vacancy immobilized Au_1 on CeO_2 (111), (c) Oxygen vacancy immobilized Au_1 on TiO_2 (101), and (d) Terminal hydroxyl bonded Au_1 on Al_2O_3 (110); AC-HAADF-STEM images for (e) Au_1/ZrO_2, (f) Au_1/CeO_2, (g) Au_1/TiO_2 and (h) Au_1/Al_2O_3. The insets in Figure 1e-1h show the percent evolution of oxygen vacancies (Vo) and coordinatively unsaturated metal ions ($Zr^{3+,}$ Ce^{3+}, Ti^{3+}) for the catalysts before and after Au insertion based on XPS deconvolution (Figure S5-S7).

First, DFT calculations were employed to build the optimized structure of four ADCs models (Figure 1a-1d, Figure S1). DFT modeling results in Figure 1a, 1b, and Figure S1a, S1b show that Au atom immobilized at Zr or Ce vacancy (adjacent to Vo) on ZrO_2 (-4.61 eV) or CeO_2 (-3.99 eV) is more thermodynamically favorable than those at oxygen vacancy (Vo) site (-3.81 eV and -2.99 eV, respectively). For TiO_2 support (Figure 1c and Figure S1c), Vo facilitates the formation of Au-Ti microstructure, with a much lower formation energy (-3.1 eV) than perfect TiO_2 (-0.42 eV, -0.37, and -0.13 eV) (see details in supporting information). Au atom at Al_2O_3 is more favorably anchored by the terminal hydroxyl (-1.11 eV) rather than lattice oxygen adsorption (-0.85 eV) (Figure d1 and Figure S1d). For catalyst synthesis, we used very low Au loading (≤ 0.04 wt% determined by ICP-OES) to ensure all Au atoms are atomically dispersed (Table S1). The dispersion of Au atom on the various oxide supports was confirmed by aberration-corrected high angle annular dark field scanning transmission electron microscopy (AC-HAADF-STEM) in Figure 1e-1h, and Figure S2. The bright spots corresponding to Au atoms are well distributed on the supports. No Au nanocluster formation was detected by further AC-HAADF-STEM examinations (*Figure S3*). We also examined more low- and high-magnification images of the different regions of the four catalysts, which confirmed that no Au atom aggregates and only single Au atoms were present in the catalysts. X-ray diffraction (XRD) analysis (*Figure S4*) also confirmed that there were no additional diffraction lines attributed to the aggregated Au nanoparticles. X-ray absorption near-edge structure (XANES) spectra (Figure S5) reveal different ionic $Au^{\delta+}$ ($0<\delta\leq1$) nature of dispersed Au atoms for four catalysts, indicating the various coordination microenvironments of Au atoms. The above results show that four Au prototype ADCs are dominated by atomically dispersed Au atoms with different coordination microenvironments.

Secondly, X-ray photoelectron spectroscopy (XPS) and electron paramagnetic resonance (EPR) were used to study the single metal atom-support interaction and the surface chemical states of these as-synthesized ADCs. **1)** For the reducible supports of ZrO_2 and CeO_2, favorable Au atoms anchoring onto cation vacancy results in an increase in the amount of unsaturated coordinated cations (Zr^{3+}/Ce^{3+}) and oxygen vacancies in Au_1/ZrO_2 and Au_1/CeO_2 due to surface restructuring [19–23,41,49,50,52] (the insets of Figure 1e and 1f; *Figure S6-S7 and Table S2*). Furthermore, the increased EPR signals corresponding to Zr^{3+} (g=1.996)[63–66] and Ce^{3+} (g=1.97 and 1.94)[67,68] and single electron trapped-oxygen vacancy (Vo·, g=2.05/2.02)[68–71] further confirmed this conclusion. In addition, the reduced line width of characteristic EPR signal for Zr^{3+} (g=1.996, Au_1/ZrO_2) and Ce^{3+} (1.97, Au_1/CeO_2) compared to their blank supports substantiate the transition of electronic microenvironment/electron coupling state, implying electronic structure modulation of support atoms by Au atom doping.[72] **2)** For the second type of reducible support of TiO_2, it is notable that Au atom insertion decreased the concentration of surface Ti^{3+} and Vo (the inset of Figure 1g, *Figure S8 and Table S2*), implied by the decreased deconvoluted area (Vo and Ti^{3+}) of XPS subpeaks and weakened intensity of EPR characteristic signals (Ti^{3+}, g=1.94 and Vo·, g=2.008).[73–75] This is due to the immobilization of Au atom predominantly situated at the location of oxygen vacancy.[30,31,37,52] **3)** For the irreducible support of Al_2O_3, the Au anchoring have no noticeable effects on chemical state of Al_2O_3 surface, with the evidence of similar binding energy of Al 2p and relatively isotropy electron density around oxygen atoms (*Figure S9a and S9b*), [76,77] as well as the absence of characteristic signal (g=2.001) assigned to Vo· (*Figure S9c*). This is consistent with DFT modeling result that single metal atoms are favorably anchored by terminal hydroxyl of Al_2O_3.[26–28] *Scheme S1* summarized the variations of coordination microenvironment for the single Au atoms: immobilized Au adjacent to oxygen vacancies (ZrO_2 and CeO_2 as supports); immobilized Au situated at oxygen vacancy (TiO_2 as support) and anchored Au by terminal hydroxyl (Al_2O_3 as support). We thus concluded that three types of Au-ensemble pool sites (Au-Vo-Zr^{3+} or Au-Vo-Ce^{3+}, Ti-Au-Ti, and Au-O) are successfully synthesized.

Au-ensemble pool sites determined ethanol dehydrogenation

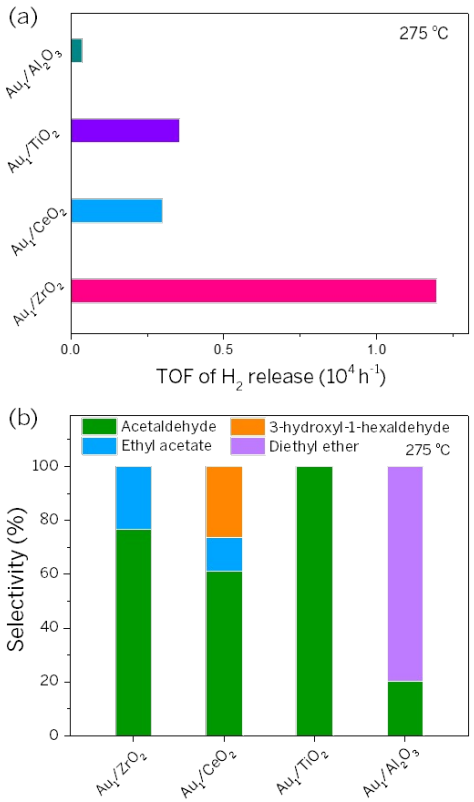

Figure 2. Au-ensemble pool site-sensitive ethanol dehydrogenation. (a) Turnover Frequency (TOF) of hydrogen release, and (b) liquid product distribution during ethanol dehydrogenation at 275 °C over Au_1/ZrO_2, Au_1/CeO_2, Au_1/TiO_2, and Au_1/Al_2O_3 ADCs.

Thirdly, we further explored the effects of various Au-ensemble pool sites (EPS) on ethanol dehydrogenation. At 275 °C, Au_1/ZrO_2 displayed a TOF of ~11948 h^{-1} for H_2 release, which is 3.37-fold, 4.01-fold and 32.0-fold higher than those of Au_1/TiO_2 (~3544 h^{-1}), Au_1/CeO_2 (~2983 h^{-1}) and Au_1/Al_2O_3 (373 h^{-1}), respectively (Figure 2a). This suggests Au-Vo-Zr^{3+} in Au_1/ZrO_2 is the optimal EPS for H_2 production. We also studied the product distributions of ethanol dehydrogenation catalyzed by these Au-EPS (Figure 2b). The major products of Au_1/ZrO_2 and Au_1/CeO_2 catalysts are acetaldehyde and ethyl acetate. For Au_1/CeO_2 catalyst, certain C_6 products (3-hydroxyal-1-hexaldehyde) were also detected. Notably, the dominant product of Au_1/TiO_2 catalyst is acetaldehyde and the major product of Au_1/Al_2O_3 is diethyl ether. The critical role of Au site in catalysis is also confirmed by catalytic results on blank oxide supports (*Figure S10*), in which Au immobilization fundamentally changed the activity and selectivity of ethanol dehydrogenation except on Al_2O_3. We hypothesized this catalytic performance difference in ADCs is assigned to their specific compositions and arrangements of Au-EPS. We also found that a higher reaction temperature favors the ethanol conversion and H_2 generation (*Figure S11a*). For example, further increasing the reaction temperature to 350 °C, the TOF of H_2 release for Au_1/ZrO_2 reaches 37,964 h^{-1}. We noticed that higher temperature triggers the generation of

complex liquid products such as C_4 (crotyl alcohol) and C_6 (hexaldehyde, heptanone) products which significantly decreases the selectivity of acetaldehyde (*Figure S11b, Table S3 and Scheme S2*). For the gas products, a trace amount of ethylene (originated from intramolecular dehydration of ethanol) was detected above 350 °C with no detectable CH_4 or CO, indicating no C-C bond cleavage and decarbonylation.[78] We further studied the stability of Au_1/ZrO_2 catalyst (*Figure S11c*). As expected, the catalyst displayed better stability under reaction temperature of 275 °C but with a relatively lower H_2 productivity than those at higher temperature reaction (300 and 350 °C).

From the above catalytic performance difference, we conclude that: 1) inserting single Au atoms on supports of ZrO_2 and CeO_2 helps create similar Au-Vo-undercoordinated metal ion (Zr^{3+} or Ce^{3+}) EPS. We propose that these EPS have similar functionality and can facilitate ethanol dehydrogenation to acetaldehyde and ethyl acetate as major products. Additionally, Au_1/ZrO_2 is proved as the optimal ethanol dehydrogenation catalyst for H_2 production; 2) loading single Au atoms on TiO_2 prefers to form Ti-Au-Ti EPS due to the Au atom favorably anchoring on the oxygen vacancy, and selectively produce acetaldehyde through ethanol dehydrogenation; 3) loading single Au atoms onto the irreducible support of Al_2O_3 by favorably stabilizing Au atoms with terminal hydroxyl does not create an obvious synergy between Au and the support atoms to form effective EPS, therefore it displays much lower dehydrogenation activity, and it is proven that the products of diethyl ether was produced by Al_2O_3 support (*Figure S9*).[79,80]

Synergistic effect of Au-Vo-Zr^{3+} EPS

After demonstrating Au-EPS-dependent ethanol dehydrogenation performance, we then used Au_1/ZrO_2 as primary prototype catalyst, combining with *in-situ* diffuse reflectance infrared Fourier transform spectra (DRIFTS), ambient pressure (AP)-XPS and EPR to study its EPS synergy in highly-sensitive ethanol dehydrogenation.

Figures 3a and 3b show the *in-situ* DRIFT spectra of Au_1/ZrO_2 and ZrO_2 samples with purging ethanol vapor in N_2 under 250 °C. After ethanol adsorption, the C-H stretching vibration bands (~2800-3000 cm^{-1}) and C-O stretching vibration bands (~1000-1200 cm^{-1}) are detected (See detailed bands assignments in *Table S4*). Especially, C-O stretching vibration can be used to identify the structure of adsorbed ethanol and adsorbed ethoxy species: for blank ZrO_2 sample, the bands at 1150, 1071 and 1050 cm^{-1} in Figure 3a are attributed to molecularly adsorbed ethanol and linearly adsorbed ethoxy species (type *a* or *b*), bridged adsorbed ethoxy species (type *c*) and bridged ethoxy adsorbed on oxygen vacancy (type *d*), respectively (*Scheme S3*).[81–89] For Au_1/ZrO_2, the enhanced adsorption peak at 1050 cm^{-1} (type *d* species) with a relatively weakened adsorption of the other types (1150 and 1071 cm^{-1}) are detected, which indicates Au atoms insertion favored the formation of type-*d* ethoxy species on the Zr^{3+} in the Au-Vo-Zr^{3+} EPS. The ethanol adsorption on Au_1/ZrO_2 is also probed by EPR (*Figure S12*). The decreased intensity of EPR characteristic signal associated with Vo is detected, which further validates the FTIR analysis that ethoxy is favorable to bind on Zr^{3+} ions surrounding Au-Vo sites. Furthermore, compared to ZrO_2, a slight red-shift of C-H stretching vibration frequencies to 2962 and 2920 cm^{-1} are observed for Au_1/ZrO_2, which indicates ethoxy adsorption at undercoordinated Zr^{3+}-Vo sites [90,91] most likely due to Au atom insertion. More interestingly, a visible band at 1758 and 1720 cm^{-1} assigned to ν(C=O) mode of acetaldehyde (Figure 3a) in the gas phase and adsorbed acetaldehyde in η^1(O)-configuration was observed. [78,83,86,92–94] We further studied the desorption dynamics of the acetaldehyde and other intermediates species on Au_1/ZrO_2 (Figure 3b). After purging with pure N_2 (without ethanol vapor), type *c* and *d* ethoxy species (1071 and

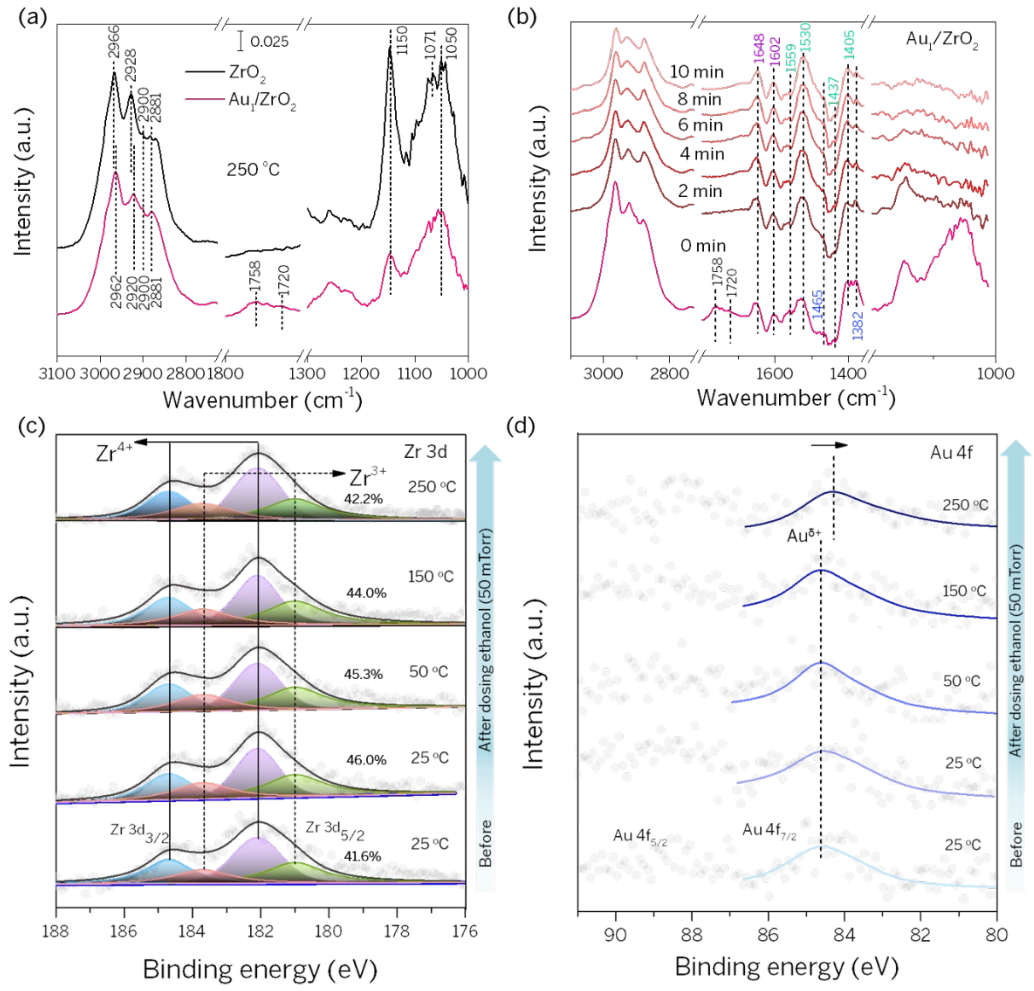

Figure 3. Spectroscopic studies on ethanol dehydrogenation over Au_1/ZrO_2. (a) In-situ diffuse reflectance infrared Fourier transform (DRIFT) spectra of Au_1/ZrO_2 and ZrO_2 when flowing ethanol vapor and N_2 at 250 ℃; (b) Time-resolved in-situ DRIFTS of Au_1/ZrO_2 in N_2 after exposure to ethanol; In–situ AP-XPS (a) Zr 3d and (b) Au 4f spectra for Au_1/ZrO_2 before and after ethanol dosing.

1050 cm^{-1}) and acetaldehyde species (1758 and 1720 cm^{-1}) are significantly decayed in 2 minutes; While the decay of molecularly adsorbed ethanol and linearly adsorbed ethoxy species (1150 cm^{-1}) is much slower than bridged ethoxy adsorbed ethoxy species. This indicates bridged deprotonated ethoxy species generated at Au-Vo-Zr^{3+} EPS or Zr^{3+}-Vo-Zr3+ are more active than others. The adsorbed crotonaldehyde species (1648 and 1602 cm^{-1}) and acetate species (1559 to 1382 cm^{-1}) are also detected, which have a much slower desorption rate. Correlated with sluggish dynamic features of ethoxy activation/reaction on blank ZrO_2 support (see detailed analyses in *Figure S13*), *in-situ* DRIFTS suggests the formation of Au-Vo-Zr^{3+} EPS enabled much higher C-H cleavage efficiency and more favorable acetaldehyde desorption properties, which explained highly efficient and selective ethanol dehydrogenation on Au_1/ZrO_2.

After resolving surface species evolution from *in-situ* DRIFTS, we conducted *In-situ* AP-XPS study to further monitor the chemical state evolution of Au_1/ZrO_2 catalyst surface during the reaction (Figure 3c and 3d). AP-XPS Zr 3d spectra in Figure 3c shows that ethanol dosing at 25 ℃ increased the amount of Zr^{3+} species mainly due to the ethoxy species with strong electron-donating capability adsorb on Zr^{4+} site and thus decreased its chemical states. A slight decrease of Zr^{3+} species from 25 to 50 ℃ is likely resulting from the ethoxy species desorption.[95,96] Interestingly, the ethanol vapor dosing has no obvious influence on the state of Au species at 84.6 eV (assigned to $Au^{\delta+}$, $0 < \delta < +1$), indicating that the Au site did not participate in the adsorption and initial activation (deprotonation) of ethanol to ethoxy species. The dehydrogenation of ethoxy species involving the α-C-H bond cleavage through H abstraction by Au atom (validated by DFT calculations in Figure 4 below) initially occurs at 150 ℃ and displays decent activity under 250 ℃ (*Figure 11a*). An obvious decrease in the amount of Zr^{3+} species for Au_1/ZrO_2 was detected at 150 and 250 ℃ (Figure 3c), due to the faster desorption of ethoxy species and its transformation to acetaldehyde species. The Au 4f binding energy of $Au^{\delta+}$

species shows a slight decrease from 150 to 250 °C (Figure 3d), resulting from the reduction effect of abstracted H species and electron-donating effect of acetaldehyde species after a substantial amount of α-C-H bond cleavage. The above analysis shows that the inter-site synergy of the Au-Vo-Zr^{3+} EPS is crucial for ethanol adsorption, activation, reaction, and desorption.

Ensemble pool synergy-mediated ethane dehydrogenation

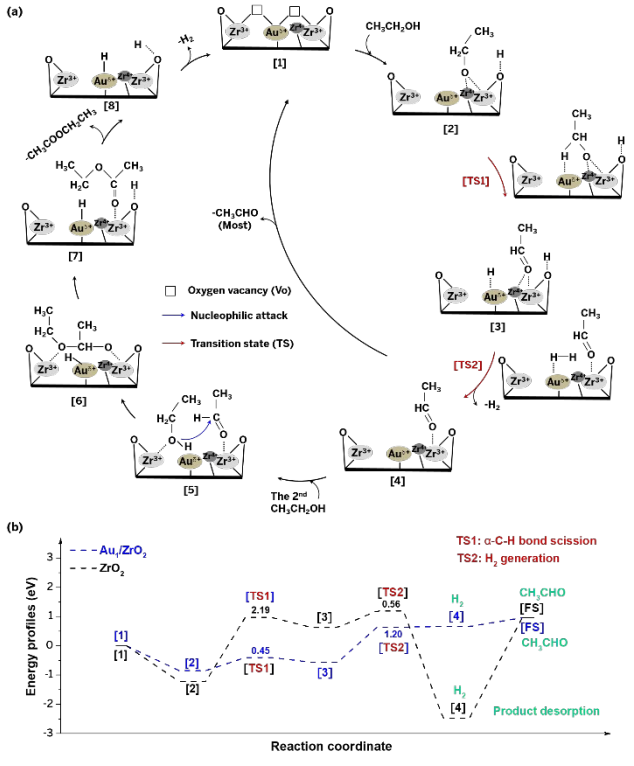

Figure 4. Zr^{3+}-Vo-$Au^{\delta+}$ mediated ensemble pool synergistic mechanism of ethanol dehydrogenation on Au_1/ZrO_2. (a) Catalytic cycle simulations of ethanol dehydrogenation on Au_1/ZrO_2. (b) The calculated energy profiles of ethanol dehydrogenation to acetaldehyde on Au/ZrO_2 and ZrO_2.

By employing DFT calculations, supported by the insights from preceding results, we developed an ensemble pool synergistic mechanism for ethanol dehydrogenation over Au_1/ZrO_2 catalyst (Figure 4, Figure S14-S16). Figure 4a shows that the catalytic cycle is initiated with the ethanol dissociation adsorption at adjacent Zr^{3+}-Vo-Zr^{4+} sites to form bridged-ethoxy-species and Zr-OH ([1] → [2]), then the scission of α-C-H bond (0.45 eV) through H abstraction by Au atom to Au-H hydride ([2] → [3]), followed by H_2 recombination (1.20 eV) and desorption ([3] → [4]), and finally acetaldehyde desorption (0.3 eV) ([4] → [1]). The catalytic cycle of ethanol dehydrogenation to acetaldehyde on Au_1/ZrO_2 is easily closed by this route with low energy. In the next stage, un-desorbed acetaldehyde intermediates would be further attacked by newly adsorbed ethanol species at Zr^{3+} ([4] → [5]) to generate ethoxy hemiacetal bridged adsorbed at two Zr atoms ([5] → [6]), followed by the decomposition of ethoxy hemiacetal to ethyl acetate (EA) intermediates at Zr site (0.12 eV) and adjacent Zr-OH ([6] → [7]). Finally, after EA desorption (0.66 eV) and H_2 formation/release ([7] → [8]), the catalytic cycle of ethanol dehydrogenation to EA is accomplished. The energy of EA desorption (0.66 eV) is 0.36 eV higher than acetaldehyde desorption (0.30 eV), indicating the thermodynamic unfavorability of reaction pathway to generate EA. This explains why acetaldehyde is the major product (with selectivity of >75%) from ethanol dehydrogenation on Au_1/ZrO_2 observed in Figure 2b.

The simulated catalytic cycle of ethanol dehydrogenation on ZrO_2 is shown in Figure S15, and the calculated energy profiles for ethanol dehydrogenation to acetaldehyde and EA over Au_1/ZrO_2 and ZrO_2 are presented in Figure 4b and Figure S16, respectively. The rate-determining step for ethanol dehydrogenation to form acetaldehyde intermediates on ZrO_2 is the cleavage of α-C-H bond (2.19 eV). With Au atom insertion into ZrO_2 to form Au-Vo-Zr^{3+} EPS, the rate-determining step on Au_1/ZrO_2 is shifted from α-C-H bond cleavage (0.45 eV) to H_2 formation with energy barrier of 1.20 eV, which is 0.99 eV lower than that of α-C-H bond scission on ZrO_2 (Table S5). Moreover, Au_1/ZrO_2 exhibited much lower energy for acetaldehyde desorption (0.3 eV vs. 3.39 eV) and EA formation (0.12 eV vs. 2.55 eV) than ZrO_2 (Table S6). Therefore, the kinetically and thermodynamically favorable elementary steps in the catalytic cycle of ethanol dehydrogenation result in the excellent catalytic performance of Au_1/ZrO_2. Its superior ethanol dehydrogenation performance is due to specific ensemble pool synergy among Zr^{3+}, oxygen vacancy and Au site.

Compared with Au_1/ZrO_2 catalyst, the Au_1/CeO_2 also contains a favorably formed Au-Vo-Ce^{3+} EPS, which is supposed to display a similar reaction pathway of ethanol dehydrogenation and product distribution. The difference between Au_1/ZrO_2 and Au_1/CeO_2 is that CeO_2-based catalyst favors further aldol condensation to produce more complicated products by surface strong basic sites on CeO_2 support.[97,98], which also prevents ethoxy dissociative adsorption through deprotonation at acid site and thus reduces ethanol dehydrogenation rate. Comparatively, the Au_1/TiO_2 catalyst preferentially creates a Ti-Au-Ti EPS which may favor the adsorption of ethanol over acid site Ti^{4+} and further dehydrogenation over Au site due to their proximity. However, it likely fails to provide a sufficient space to adsorb another ethoxy for further reaction with acetaldehyde to generate ethoxy hemiacetal since Au-Ti are adjacent to each other. Therefore, Au_1/TiO_2 catalyst produces acetaldehyde as the final product with 100 % selectivity. Compared with Au_1/ZrO_2 catalyst, the formation of Au_1/TiO_2 catalyst does not create extra Ti^{3+} after Au immobilization, and the limited Ti^{3+} amount may account for its lower activity than Au_1/ZrO_2 catalyst. The Au_1/Al_2O_3 catalyst displays the lowest H_2 generation rate and the highest diethyl ether selectivity, which is due to the absence of inter-site synergy between Au and Al^{3+}

site. Here, the diethyl ether is generated over the surface of Al_2O_3, which further demonstrates the poor activity of its Au site. More computation research to explore optimal ensemble pool synergy on ethanol dehydrogenation is ongoing in our lab.

Conclusion

In summary, we demonstrated Au-EPS-sensitive ethanol dehydrogenation in atomically dispersed gold catalysts with irreducible and reducible oxides (Al_2O_3, ZrO_2, CeO_2, and TiO_2) as supports and unraveled ensemble pool catalysis synergy mechanism. The EPS composed of predominant Au-Vo-Zr^{3+} or Au-Vo-Ce^{3+} complex for Au_1/ZrO_2 or Au_1/CeO_2 facilitates ethanol dehydrogenation to produce acetaldehyde and ethyl acetate as major products. The Au_1/TiO_2 catalyst favorably creates Ti-Au-Ti EPS which favors the acetaldehyde production with 100 % selectivity. The Au_1/Al_2O_3 catalyst with Au atom stabilized by terminal hydroxyl lacks Au_1-support atoms ensemble synergy and initiates ethanol dehydration to generate the main product of diethyl ether. Moreover, Au_1/ZrO_2 exhibited the highest H_2 production rate from ethanol dehydrogenation among these catalysts. In-situ DRIFTS, APXPS, and DFT calculation results show that this exceptional catalytic performance is assigned to the specific ensemble pool synergy among Au^{6+}-Vo-Zr^{3+}. Vo-Zr^{3+} facilitates ethanol diccociative adsorption to generate active ethoxy, and adjacent Au site facilitate α-C-H bond cleavage through H abstraction, followed by fast product desorption on Vo-Zr^{3+}, which enabled kinetically and thermodynamically favorable elementary steps, thus efficiently and selectively facilitating ethanol dehydrogenation. This work highlights the advantages of ensemble pool site by engineering metal atom microenvironment in ADCs, and provides new perspectives on the synthesis of atomically synergistic site catalysts by exploiting support atoms and surface functional species. The mechanistic insights revealed as ensemble-pool synergy here also provide a deep understanding of atomically synergistic site formation.

Acknowledgments

This work was financially supported by the Hydrogen Materials Advanced Research Consortium (HyMARC), established as part of the Energy Materials Network by the U.S. Department of Energy, Office of Energy Efficiency and Renewable Energy, Fuel Cell Technologies Office, under Contract Number DE-AC02-05CH11231. Spectroscopic and microscopic experiments were performed at the Advanced Light Source (ALS) and Molecular Foundry at LBNL under contract no. DE-AC02-05CH11231. Ji Yang acknowledges the China Scholarship Council for providing his exchange scholarship.

AUTHOR CONTRIBUTIONS

J. S., Y. G., J. J. U., and G. A. S. designed research; J. Y., J. Z., and C. D. performed research; J. Y., J. Z., C. D., L. J. F., Q. Z., J. C., M. Z., N. J., C. A., J. G., M. S., and D. P. analyzed data; and J. Y., J. Z., and C. D., G. A. S., J. J. U., Y. G., and J. S. wrote the paper.

DECLARATION OF INTERESTS

The authors declare no competing interests.

Keywords: Gold atom; Ensemble pool sites; Ensemble-pool synergy; Atomically dispersed catalysts; Ethanol dehydrogenation

[1] U. Eberle, M. Felderhoff, F. Schüth, *Angew. Chem. Int. Ed.* **2009**, *48*, 6608–6630.

[2] C. Mevawala, K. Brooks, M. E. Bowden, H. M. Breunig, B. L. Tran, O. Y. Gutiérrez, T. Autrey, K. Müller, *Energy Technol.* **2023**, *11*, 1–8.

[3] B. L. Tran, S. I. Johnson, K. P. Brooks, S. T. Autrey, *ACS Sustain. Chem. Eng.* **2021**, *9*, 7130–7138.

[4] S. Ji, Y. Chen, X. Wang, Z. Zhang, D. Wang, Y. Li, *Chem. Rev.* **2020**, *120*, 11900–11955.

[5] R. Qin, K. Liu, Q. Wu, N. Zheng, *Chem. Rev.* **2020**, *120*, 11810–11899.

[6] J. Jones, H. Xiong, A. T. DeLaRiva, E. J. Peterson, H. Pham, S. R. Challa, G. Qi, S. Oh, M. H. Wiebenga, X. I. P. Hernández, Y. Wang, A. K. Datye, *Science 80.* **2016**, *353*, 150–154.

[7] J. Shan, M. Li, L. F. Allard, S. Lee, M. Flytzani-Stephanopoulos, *Nature* **2017**, *551*, 605–608.

[8] P. Liu, Y. Zhao, R. Qin, S. Mo, G. Chen, L. Gu, D. M. Chevrier, P. Zhang, Q. Guo, D. Zang, B. Wu, G. Fu, N. Zheng, *Science* **2016**, *352*, 797–801.

[9] Y. Li, Y. Zhang, K. Qian, W. Huang, *ACS Catal.* **2022**, *12*, 1268–1287.

[10] Y. Li, M. Kottwitz, J. L. Vincent, M. J. Enright, Z. Liu, L. Zhang, J. Huang, S. D. Senanayake, W. C. D. Yang, P. A. Crozier, R. G. Nuzzo, A. I. Frenkel, *Nat. Commun.* **2021**, *12*, 914.

[11] A. Wang, J. Li, T. Zhang, *Nat. Rev. Chem.* **2018**, *2*, 65–81.

[12] A. J. Hoffman, C. Asokan, N. Gadinas, P. Kravchenko, A. Getsoian, P. Christopher, D. Hibbitts, *J. Phys. Chem. C* **2021**, *125*, 19733–19755.

[13] P. Tieu, J. Lee, C. Gadre, X. Yan, W. Zang, P. Christopher, X. Pan, *Microsc. Microanal.* **2022**, *28*, 2426–2428.

[14] L. DeRita, J. Resasco, S. Dai, A. Boubnov, H. V. Thang, A. S. Hoffman, I. Ro, G. W. Graham, S. R. Bare, G. Pacchioni, X. Pan, P. Christopher, *Nat. Mater.* **2019**, *18*, 746–751.

[15] C. Asokan, M. Xu, S. Dai, X. Pan, P. Christopher, *J. Phys. Chem. C* **2022**, *126*, 18704–18715.

[16] Y. Tang, C. Asokan, M. Xu, G. W. Graham, X. Pan, P. Christopher, J. Li, P. Sautet, *Nat. Commun.* **2019**, *10*, 1–10.

[17] J. Resasco, L. Derita, S. Dai, J. P. Chada, M. Xu, X. Yan, J. Finzel, S. Hanukovich, A. S. Hoffman, G. W. Graham, S. R. Bare, X. Pan, P. Christopher, *J. Am. Chem. Soc.* **2020**, *142*, 169–184.

[18] T. Zhang, *Nano Lett.* **2021**, *21*, 9835–9837.

[19] L. N. Chen, K. P. Hou, Y. S. Liu, Z. Y. Qi, Q. Zheng, Y. H. Lu, J. Y. Chen, J. L. Chen, C. W. Pao, S. B. Wang, Y. Bin Li, S. H. Xie, F. D. Liu, D. Prendergast, L. E. Klebanoff, V. Stavila, M. D. Allendorf, J. Guo, L. S. Zheng, J. Su, G. A. Somorjai, *J. Am. Chem. Soc.* **2019**, *141*, 17995–17999.

[20] Z. Qi, L. Chen, S. Zhang, J. Su, G. A. Somorjai, *J. Am. Chem. Soc.* **2021**, *143*, 60–64.

[21] S. Zhang, L. Chen, Z. Qi, L. Zhuo, J. L. Chen, C. W. Pao, J. Su, G. A. Somorjai, *J. Am. Chem. Soc.* **2020**, *142*, 16533–16537.

[22] L. Chen, Z. Qi, X. Peng, J. L. Chen, C. W. Pao, X. Zhang, C. Dun, M. Young, D. Prendergast, J. J. Urban, J. Guo, G. A. Somorjai, J. Su, *J. Am. Chem. Soc.* **2021**, *143*, 12074–12081.

[23] L. Chen, P. Verma, K. Hou, Z. Qi, S. Zhang, Y. Liu, J. Guo, V. Stavila, M. D. Allendorf, L. Zheng, M. Salmeron, D. Prendergast, G. A. Somorjai, J. Su, *Nat. Commun.* **2022**, *13*, 1092.

[24] S. Xie, L. Liu, Y. Lu, C. Wang, S. Cao, W. Diao, J. Deng, W. Tan, L. Ma, S. N. Ehrlich, Y. Li, Y. Zhang, K. Ye, H. Xin, M. Flytzani-stephanopoulos, F. Liu, *J. Am. Chem. Soc.* **2022**, DOI 10.1021/jacs.2c08902.

[25] K. Zhang, Q. Meng, H. Wu, J. Yan, X. Mei, P. An, L. Zheng, J. Zhang, M. He, B. Han, *J. Am. Chem. Soc* **2022**, *144*, 20834–20846.

[26] T. K. Ghosh, N. N. Nair, *ChemCatChem* **2013**, *5*, 1811–1821.

[27] M. Moses-Debusk, M. Yoon, L. F. Allard, D. R. Mullins, Z. Wu, X. Yang, G. Veith, G. M. Stocks, C. K. Narula, *J. Am. Chem. Soc.* **2013**, *135*, 12634–12645.

[28] F. Wang, J. Ma, S. Xin, Q. Wang, J. Xu, C. Zhang, H. He, X. Cheng Zeng, *Nat. Commun.* **2020**, *11*, 1–9.

[29] A. Beniya, S. Higashi, *Nat. Catal.* **2019**, *2*, 590–602.

[30] A. Mellor, D. Humphrey, C. M. Yim, C. L. Pang, H. Idriss, G. Thornton, *J. Phys. Chem. C* **2017**, *121*, 24721–24725.

[31] S. Dong, B. Li, X. Cui, S. Tan, B. Wang, *J. Phys. Chem. Lett.* **2019**, *10*, 4683–4691.

[32] G. Liu, A. W. Robertson, M. M. J. Li, W. C. H. Kuo, M. T. Darby, M. H. Muhieddine, Y. C. Lin, K. Suenaga, M. Stamatakis, J. H. Warner, S. C. E. Tsang, *Nat. Chem.* **2017**, *9*, 810–816.

[33] S. Yang, J. Kim, Y. J. Tak, A. Soon, H. Lee, *Angew. Chem. Int. Ed.* **2016**, *55*, 2058–2062.

[34] L. Tao, C. Y. Lin, S. Dou, S. Feng, D. Chen, D. Liu, J. Huo, Z. Xia, S. Wang, *Nano Energy* **2017**, *41*, 417–425.

[35] R. Q. Zhang, T. H. Lee, B. D. Yu, C. Stampfl, A. Soon, *Phys. Chem. Chem. Phys.* **2012**, *14*, 16552–16557.

[36] J. Wan, W. Chen, C. Jia, L. Zheng, J. Dong, X. Zheng, Y. Wang, W. Yan, C. Chen, Q. Peng, D. Wang, Y. Li, *Adv. Mater.* **2018**, *30*, 1705369.

[37] Z. Hu, C. Yang, K. Lv, X. Li, Q. Li, J. Fan, *Chem. Commun.* **2020**, *56*, 1745.

[38] Y. Lou, Y. Cai, W. Hu, L. Wang, Q. Dai, W. Zhan, Y. Guo, P. Hu, X. M. Cao, J. Liu, Y. Guo, *ACS Catal.* **2020**, *10*, 6094–6101.

[39] B. Qiao, J. X. Liang, A. Wang, C. Q. Xu, J. Li, T. Zhang, J. J. Liu, *Nano Res.* **2015**, *8*, 2913–2924.

[40] B. Qiao, A. Wang, X. Yang, L. F. Allard, Z. Jiang, Y. Cui, J. Liu, J. Li, T. Zhang, *Nat. Chem.* **2011**, *3*, 634–641.

[41] K. Harrath, X. Yu, H. Xiao, J. Li, *ACS Catal.* **2019**, *9*, 8903–8909.

[42] S. Dong, W. Liu, S. Liu, F. Li, J. Hou, R. Hao, X. Bai, H. Zhao, J. Liu, L. Guo, *Mater. Today Nano* **2022**, *17*, 100157.

[43] L. W. Guo, P. P. Du, X. P. Fu, C. Ma, J. Zeng, R. Si, Y. Y. Huang, C. J. Jia, Y. W. Zhang, C. H. Yan, *Nat. Commun.* **2016**, *7*, 13481.

[44] J. Zhang, X. Wu, W. C. Cheong, W. Chen, R. Lin, J. Li, L. Zheng, W. Yan, L. Gu, C. Chen, Q. Peng, D. Wang, Y. Li, *Nat. Commun.* **2018**, *9*, 1–8.

[45] S. Ida, N. Kim, E. Ertekin, S. Takenaka, T. Ishihara, *J. Am. Chem. Soc.* **2015**, *137*, 239–244.

[46] S. Zhao, F. Chen, S. Duan, B. Shao, T. Li, H. Tang, Q. Lin, J. Zhang, L. Li, J. Huang, N. Bion, W. Liu, H. Sun, A. Q. Wang, M. Haruta, B. Qiao, J. Li, J. Liu, T. Zhang, *Nat. Commun.* **2019**, *10*, 1–9.

[47] L. W. Guo, P. P. Du, X. P. Fu, C. Ma, J. Zeng, R. Si, Y. Y. Huang, C. J. Jia, Y. W. Zhang, C. H. Yan, *Nat. Commun.* **2016**, *7*, 13481.

[48] B. Han, R. Lang, H. Tang, J. Xu, X. K. Gu, B. Qiao, J. Liu, *Chinese J. Catal.* **2019**, *40*, 1847–1853.

[49] B. Qiao, J. Liu, Y. G. Wang, Q. Lin, X. Liu, A. Wang, J. Li, T. Zhang, J. Liu, *ACS Catal.* **2015**, *5*, 6249–6254.

[50] Z. P. Liu, C. M. Wang, K. N. Fan, *Angew. Chem. Int. Ed.* **2006**, *45*, 6865–6868.

[51] L. DeRita, S. Dai, K. Lopez-Zepeda, N. Pham, G. W. Graham, X. Pan, P. Christopher, *J. Am. Chem. Soc.* **2017**, *139*, 14150–14165.

[52] J. Wan, W. Chen, C. Jia, L. Zheng, J. Dong, X. Zheng, Y. Wang, W. Yan, C. Chen, Q. Peng, D. Wang, Y. Li, *Adv. Mater.* **2018**, *30*, 1705369.

[53] Y. Xie, J. Chen, X. Wu, J. Wen, R. Zhao, Z. Li, G. Tian, Q. Zhang, P. Ning, J. Hao, *ACS Catal.* **2022**, *12*, 10587–10602.

[54] S. Zhang, Z. Q. Huang, Y. Ma, W. Gao, J. Li, F. Cao, L. Li, C. R. Chang, Y. Qu, *Nat. Commun.* **2017**, *8*, 1–11.

[55] S. Zhang, Z. Xia, Y. Zou, F. Cao, Y. Liu, Y. Ma, Y. Qu, *J. Am. Chem. Soc* **2019**, *141*, 11353–11357.

[56] Y. Ma, S. Zhang, C. R. Chang, Z. Q. Huang, J. C. Ho, Y. Qu, *Chem. Soc. Rev.* **2018**, *47*, 5541–5553.

[57] Z. Wu, Y. Cheng, F. Tao, L. Daemen, G. S. Foo, L. Nguyen, X. Zhang, A. Beste, A. J. Ramirez-Cuesta, *J. Am. Chem. Soc.* **2017**, *139*, 9721–9727.

[58] T. Livneh, D. Avisar, *J. Phys. Chem. C* **2020**, *124*, 28018–28025.

[59] Y. Jiang, O. Blacque, T. Fox, H. Berke, *J. Am. Chem. Soc.* **2013**, *135*, 7751–7760.

[60] X. Zhang, G. Liu, K. H. Meiwes-Broer, G. Ganteför, K. Bowen, *Angew. Chem. Int. Ed.* **2016**, *55*, 9644–9647.

[61] A. Álvarez, M. Borges, J. J. Corral-Pérez, J. G. Olcina, L. Hu, D. Cornu, R. Huang, D. Stoian, A. Urakawa, *ChemPhysChem* **2017**, *18*, 3135–3141.

[62] J. Yang, F. Liang, Y. Cheng, D. Yin, L. Wang, *Int. J.*

Hydrog. Energy **2020**, *45*, 2119–2126.
[63] F. R. Chen, G. Coudurier, J. F. Joly, J. C. Vedrine, *J. Catal.* **1993**, *143*, 616–626.
[64] C. R. Vera, C. L. Pieck, K. Shimizu, C. A. Querini, J. M. Parera, *J. Catal.* **1999**, *187*, 39–49.
[65] J. Huang, J. Liu, L. Tian, X. Li, X. Ma, X. Yu, Q. Guo, J. Zhao, *Chem. Eng. J.* **2021**, *412*, 128621.
[66] J. M. Costantini, F. Beuneu, *Phys. Stat. Sol.* **2007**, *4*, 1258–1263.
[67] R. A. Elsalamony, D. R. Abd El-Hafiz, M. A. Ebiad, A. M. Mansour, L. S. Mohamed, *RSC Adv.* **2013**, *3*, 23791–23800.
[68] A. A. Marciniak, F. J. F. S. Henrique, A. F. F. de Lima, O. C. Alves, C. R. Moreira, L. G. Appel, C. J. A. Mota, *Mol. Catal.* **2020**, *493*, 111053.
[69] O. E. Everett Espino, P. C. Zonetti, R. R. Celin, L. T. Costa, O. C. Alves, J. C. Spadotto, L. G. Appel, R. R. De Avillez, *Catal. Sci. Technol.* **2022**, *12*, 1324–1338.
[70] E. Mamontov, T. Egami, R. Brezny, M. Koranne, S. Tyagi, *J. Phys. Chem. B* **2000**, *104*, 11110–11116.
[71] A. A. Marciniak, O. C. Alves, L. G. Appel, C. J. A. Mota, *J. Catal.* **2019**, *371*, 88–95.
[72] E. P. Saliba, E. L. Sesti, F. J. Scott, B. J. Albert, E. J. Choi, N. Alaniva, C. Gao, A. B. Barnes, *J. Am. Chem. Soc.* **2017**, *139*, 6310–6313.
[73] E. Morra, E. Giamello, S. Van Doorslaer, G. Antinucci, M. D'Amore, V. Busico, M. Chiesa, *Angew. Chem. Int. Ed.* **2015**, *54*, 4857–4860.
[74] Q. Zhu, Y. Peng, L. Lin, C. M. Fan, G. Q. Gao, R. X. Wang, A. W. Xu, *J. Mater. Chem. A* **2014**, *2*, 4429–4437.
[75] H. Xie, N. Li, X. Chen, J. Jiang, X. Zhao, *Appl. Surf. Sci.* **2020**, *511*, 145597.
[76] K. Yang, J. Liu, R. Si, X. Chen, W. Dai, X. Fu, *J. Catal.* **2014**, *317*, 229–239.
[77] J. Xie, M. Yao, W. Gao, Z. Su, X. Yao, *J. Alloy. Compd.* **2019**, *772*, 324–331.
[78] C. Wang, G. Garbarino, L. F. Allard, F. Wilson, G. Busca, M. Flytzani-Stephanopoulos, *ACS Catal.* **2016**, *6*, 210–218.
[79] G. R. Jenness, M. A. Christiansen, S. Caratzoulas, D. G. Vlachos, R. J. Gorte, *J. Phys. Chem. C* **2014**, *118*, 12899–12907.
[80] J. F. DeWilde, H. Chiang, D. A. Hickman, C. R. Ho, A. Bhan, *ACS Catal.* **2013**, *3*, 798–807.
[81] Z. Qi, L. Chen, S. Zhang, J. Su, G. A. Somorjai, *J. Am. Chem.Soc.* **2021**, *143*, 60–64.
[82] J. Cornejo-Romero, A. Solis-Garcia, S. M. Vega-Diaz, J. C. Fierro-Gonzalez, *Mol. Catal.* **2017**, *433*, 391–402.
[83] S. Luo, H. Song, D. Philo, M. Oshikiri, T. Kako, J. Ye, *Appl. Catal. B Environ.* **2020**, *272*, 118965.
[84] M. Martinelli, C. D. Watson, G. Jacobs, *Int. J. Hydrog. Energy* **2020**, *45*, 18490–18501.
[85] S. Rousseau, O. Marie, P. Bazin, M. Daturi, S. Verdier, V. Harlé, *J. Am. Chem. Soc.* **2010**, *132*, 10832–10841.
[86] E. O. Gonzalez-Yañez, G. A. Fuentes, M. E. Hernández-Terán, J. C. Fierro-Gonzalez, *Appl. Catal. A Gen.* **2013**, *464–465*, 374–383.
[87] G. Jacobs, R. A. Keogh, B. H. Davis, *J. Catal.* **2007**, *245*, 326–337.
[88] M. Martinelli, J. D. Castro, N. Alhraki, M. E. Matamoros, A. J. Kropf, D. C. Cronauer, G. Jacobs, *Appl. Catal. A Gen.* **2021**, *610*, 117947.
[89] M. Martinelli, R. Garcia, C. D. Watson, D. C. Cronauer, A. J. Kropf, G. Jacobs, *Nanomaterials* **2021**, *11*, 1–24.
[90] Z. Rajabi, L. Jones, M. Martinelli, D. Qian, D. C. Cronauer, A. J. Kropf, C. D. Watson, G. Jacobs, *Catalysts* **2021**, *11*, 1104.
[91] M. Martinelli, C. D. Watson, G. Jacobs, *Int. J. Hydrogen Energy* **2020**, *45*, 18490–18501.
[92] J. Cornejo-romero, A. Solis-garcia, S. M. Vega-diaz, J. C. Fierro-gonzalez, *Mol. Catal.* **2017**, *433*, 391–402.
[93] M. B. Boucher, M. D. Marcinkowski, M. L. Liriano, C. J. Murphy, E. A. Lewis, A. D. Jewell, M. F. G. Mattera, G. Kyriakou, M. Flytzani-stephanopoulos, E. C. H. Sykes, *ACS Nano* **2013**, *7*, 6181–6187.
[94] C. Wang, M. Yang, M. Flytzani-stephanopoulos, *AIChE J.* **2016**, *62*, 429–439.
[95] A. P. Farkas, Á. Szitás, D. Jurdi, K. Palotás, J. Kiss, Z. Kónya, *Appl. Catal. A Gen.* **2020**, *592*, 117440.
[96] A. Gazsi, A. Koós, T. Bánsági, F. Solymosi, *Catal. Today* **2011**, *160*, 70–78.
[97] T. Nishiguchi, T. Matsumoto, H. Kanai, K. Utani, *Appl. Catal. A Gen.* **2005**, *279*, 273–277.
[98] M. Xu, M. J. L. Gines, A. Hilmen, B. L. Stephens, E. Iglesia, *J. Catal.* **1997**, *147*, 130–147.

Entry for the Table of Contents

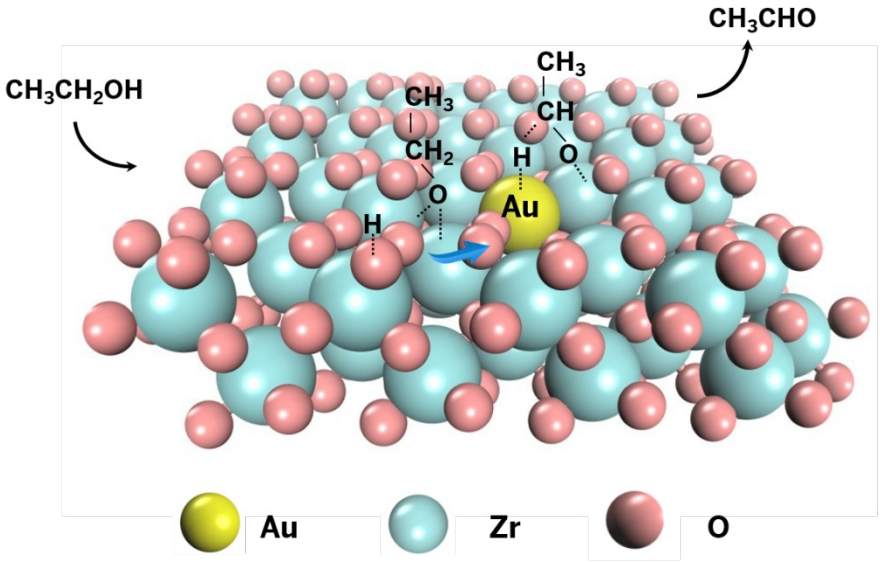

Specific ensemble pool synergy of Au-oxygen vacancy-Zr^{3+} sites facilitates distinct elementary steps and thus results in excellent ethanol dehydrogenation efficiency and selectivity.